

Forecast on $f(R)$ Gravity with HI 21cm Intensity Mapping Surveys

Yanling Song,¹ Yu Sang,^{1,*} Linfeng Xiao,² Boyu Zhang,³ and Bin Wang^{1,4}

¹*Center for Gravitation and Cosmology, College of Physical Science and Technology, Yangzhou University, Yangzhou, 225009, China*

²*Department of Physics and Astronomy, Sejong University, Seoul, 143-747, Korea*

³*Department of Astronomy, School of Physical Sciences,*

University of Science and Technology of China, Hefei, Anhui 230026, China

⁴*School of Aeronautics and Astronautics, Shanghai Jiao Tong University, Shanghai 200240, China*

Modified gravity theories offer a well-motivated extension of General Relativity and provide a possible explanation for the late-time accelerated expansion of the Universe. Among them, $f(R)$ gravity represents a minimal and theoretically appealing class, characterized by the Compton wavelength parameter B_0 , which quantifies deviations from General Relativity. In this work, we explore the capability of future neutral hydrogen (HI) 21 cm intensity mapping (IM) observations to constrain $f(R)$ gravity at low redshifts. We perform Fisher-matrix forecasts for B_0 and standard cosmological parameters using upcoming 21 cm IM experiments, including BINGO and SKA1-MID (Band 1 and Band 2), both individually and in combination with Planck cosmic microwave background (CMB) priors. We find that even near-term experiments such as BINGO are able to place nontrivial bounds on B_0 , $\sigma(B_0) \simeq 2.27 \times 10^{-6}$, while SKA1-MID yields substantially tighter constraints, with SKA Band 2 providing the strongest sensitivity among the considered configurations, $\sigma(B_0) \simeq 6.37 \times 10^{-8}$. We further demonstrate that the combination of low-redshift 21 cm IM data with CMB observations efficiently breaks degeneracies with background cosmological parameters and leads to a significant improvement in the constraints on B_0 . These results highlight the potential of future HI intensity mapping surveys, in combination with CMB measurements, to provide stringent tests of General Relativity on cosmological scales.

I. INTRODUCTION

Observations of Type Ia supernovae indicate that the Universe is undergoing accelerated expansion [1]. The Λ CDM cosmological model is the simplest explanation for the accelerated expansion and provides a good fit to most cosmological observations. However, the Λ CDM cosmological model is challenged by the inconsistent cosmological parameters inferred from different measurements. The Hubble parameter derived from cosmic microwave background (CMB) measurements is inconsistent with that from the SH0ES (Supernovae and H_0 for the EoS of DE) at the 5σ confidence level, which is called Hubble tension [2, 3]. Another tension is of σ_8 , the mass variance on a scale of $8\text{Mpc}/\text{h}$, which comes from the 3σ discrepancy between the measurements of the CMB lensing and cosmic shear surveys [3–5]. These observational tensions motivate the studies of modification of General Relativity (GR) on cosmological scales. Among the alternative theories, $f(R)$ gravity has been widely studied due to its simple form and clear physical descriptions. It is a modified gravity theory that adds a general function $f(R)$ of the Einstein-Hilbert action R , introducing a scalar degree of freedom called the scalaron that regulates gravitational interactions on cosmological scales [6–8].

A key parameter in $f(R)$ gravity is B_0 , which represents the present-day value of the Compton wavelength of the scalaron expressed in units of the Hubble length [7, 9]. This parameter quantifies the deviation of $f(R)$ gravity from GR. When $B_0 = 0$, the Λ CDM model is recovered, whereas non-zero value of B_0 indicates gravitational modifications of the expansion history of the universe and the formation of large-scale structure (LSS) [10]. Due to the limited sensitivity of observational probes, current cosmological observational data impose constraints on B_0 at order of 10^{-4} . Using CMB alone, the constraint is $B_0 < 3.37$ for WMAP9 and $B_0 < 0.18$ for Planck at 95% confidence level (C.L.) [11]. LSS probes based on galaxy clustering, cluster abundance, growth rates and galaxy power spectra place strong constraints on B_0 . Inclusion of data from cluster abundance to the measurement from supernovae, acoustic oscillation (BAO), Hubble constant and CMB, is largely improving the constraints to $B_0 < 1.1 \times 10^{-3}$ at the 95% C.L. [12]. The combination of Planck CMB data and BAO data yields tight constraints on B_0 , with $B_0 < 0.006$ at the 95% C.L. for $w = -1$, and $B_0 < 0.0045$ (95% C.L.) when $w \neq -1$ [13]. WiggleZ power spectrum in addition with CMB data from Planck give $\log_{10} B_0 < -4.07$ at 95% C.L. [14]. And cluster abundance plus CMB and BAO yields a constraints of $\log_{10} B_0 < -3.68$ at the 95% C.L. [15]. Scale-dependent growth rates of structure combined with CMB and BAO give $\log_{10} B_0 < -4.1$ at 95% C.L. [16].

* sangyu@yzu.edu.cn (corresponding author)

In addition to current high-precision measurements from CMB and galaxy survey, neutral hydrogen (HI) 21 cm intensity mapping (IM) has emerged as a powerful probe of cosmology and modified gravity in the radio waveband [17–19]. Unlike traditional galaxy surveys, 21 cm IM does not require the resolution of individual galaxies. The primary objective of HI IM is to map the integrated 21 cm radiation intensity from numerous unresolved galaxies across a given redshift range [20, 21]. This signal encodes information on matter density perturbations, redshift-space distortions (RSD), and gravitational potentials, making it sensitive to signatures of modified gravity [17]. In this work, we focus on constraining $f(R)$ gravity using 21 cm IM data from BINGO and SKA. BINGO is a single-dish telescope in Brazil, covering 3000 deg² at redshifts $0.13 \leq z \leq 0.45$ (980–1260 MHz) with an angular resolution of 40 arcmin [22–30]. SKA1-MID is a dish array in South Africa, operating in two bands: Band 1 (350–1050 MHz, $0.36 \leq z \leq 3.0$) covering 20000 deg² and Band 2 (950–1410 MHz, $0.01 \leq z \leq 0.49$) covering 5000 deg², with significantly lower system temperatures (15 K for Band 2) than BINGO (70 K) [31]. These experiments can further reduce noise and are expected to place tight constraints on $f(R)$ gravity.

In this work, we forecast the constraints on B_0 using 21 cm IM from BINGO and SKA1-MID, combined with CMB observations. In Section II, we introduce the $f(R)$ gravity, with its background and perturbation evolutions. In Section III, we describe the redshifted 21 cm HI signal in the framework of $f(R)$ gravity, including the brightness temperature evolutions at the background and perturbation level. We also include the angular power spectrum of the HI signal. In Section IV, we present the thermal and shot noise for each experiment, and using the Fisher matrix method to forecast constraints on B_0 and key cosmological parameters. In Section V we show the results and in Section VI we present the conclusions.

II. F(R) GRAVITY MODELS

We focus on the following action in Jordan frame given by

$$S = \frac{1}{16\pi G} \int d^4x \sqrt{-g} (R + f(R)) + S_m, \quad (1)$$

where g is the determinant of the metric, R is the Ricci scalar and $f(R)$ is an arbitrary function of R , S_m is the action for matter fields. Taking the variation of the above action with respect to the metric, one get the modified Einstein equations [32–34]:

$$G_{\alpha\beta} + f_R R_{\alpha\beta} - \left(\frac{f}{2} - \square f_R\right) g_{\alpha\beta} - \nabla_\alpha \nabla_\beta f_R = \kappa^2 T_{\alpha\beta}, \quad (2)$$

where $f_R = df(R)/dR$, $\kappa^2 = 8\pi G$. When giving the flat FLRW metrc $ds^2 = a^2(\tau)(d\tau^2 - d\vec{x}^2)$, one can get the background evolutions [32, 34, 35]:

$$(1 + f_R)\mathcal{H}^2 + \frac{a^2}{6}f - \frac{\ddot{a}}{a}f_R + \mathcal{H}\dot{f}_R = \frac{\kappa^2}{3}a^2\rho \quad (3)$$

$$\frac{\ddot{a}}{a} - (1 + f_R)\mathcal{H}^2 + \frac{a^2}{6}f + \frac{1}{2}\ddot{f}_R = -\frac{\kappa^2}{6}a^2(\rho + 3P) \quad (4)$$

where $\mathcal{H} = \dot{a}/a$, and an overdot denotes differentiation with respect to conformal time. Since f is an arbitrary function of R , the background evolutions can be tunned to fit any kinds of Λ CDM or non- Λ CDM histories. And we define the Compton wavelength of the scalaron in Hubble units [32]:

$$B = \frac{f_{RR}}{1 + f_R} \frac{\mathcal{H}\dot{R}}{\dot{\mathcal{H}} - \mathcal{H}^2}. \quad (5)$$

One can find a family of f forms for the fitting of a given expansion history through B 's present value B_0 , or equivalently, through the boundary condition f_R^0 . In Λ CDM case, B_0 can be related to f_R^0 approximately by $B_0 \approx -6f_R^0$ [36].

For perturbations, we consider scalar perturbations in the Newtonian gauge, with the line element given by

$$ds^2 = a^2[(1 + 2\Psi)d\tau^2 - (1 - 2\Phi)d\vec{x}^2], \quad (6)$$

and the perturbed energy-momentum tensor is

$$\begin{aligned} T_0^0 &= -\rho(1 + \delta), \\ T_i^0 &= -(\rho + P)v_i, \\ T_i^j &= (P + \delta P)\delta_i^j, \end{aligned} \quad (7)$$

where $\delta = \delta\rho/\rho$ is the density contrast, v is the velocity, δP the pressure perturbation, $\delta_i^j = 0$ for $i \neq j$ and $\delta_i^j = 1$ for $i = j$. In the Jordan frame, the metric $g_{\mu\nu}$ is minimally coupled to matter, so the energy-momentum is conserved. And the continuity and Euler equations retain their forms as in the standard GR, in Fourier space, they become [17]

$$\dot{\delta} + kv - 3\dot{\Phi} = 0, \quad (8)$$

$$\dot{v} + \mathcal{H}v - k\Psi = 0. \quad (9)$$

Then one can see that the differences under modified gravities for δ, v is depicted in Φ, Ψ . For the full set of perturbation equations, one can submit equations (6) and (7) to solve for the modified Einstein equations. One can refer to Ref. [34] for the explicit expression of these equations. Here we want to focus on the effective anisotropy and the modified Poisson equations that generally describe the deflections of modified gravities from GR. As in MGCBM [37], the modification to Poisson and anisotropy equations are encoded in two functions $\mu(a, k)$ and $\gamma(a, k)$ defined by

$$k^2\Psi = -\frac{a^2}{2M_{pl}^2}\mu(a, k)\rho\Delta, \quad (10)$$

$$\frac{\Phi}{\Psi} = \gamma(a, k), \quad (11)$$

where M_{pl} is the Planck mass, and $\rho\Delta = \rho\delta + 3\frac{aH}{k}(\rho + P)v$ is the comoving density perturbation. On quasi-static scales the B_0 parameterization of f(R) gravity can be parameterized by [28, 38, 39]

$$\mu(a, k) = \frac{1}{1 - 1.4 \times 10^{-8}|\lambda/\text{Mpc}|^2 a^3} \frac{1 + \frac{4}{3}\lambda^2 k^2 a^4}{1 + \lambda^2 k^2 a^4}, \quad (12)$$

$$\gamma(a, k) = \frac{1 + \frac{2}{3}\lambda^2 k^2 a^4}{1 + \frac{4}{3}\lambda^2 k^2 a^4}, \quad (13)$$

where $B_0 = 2H_0^2\lambda^2$.

III. 21CM ANGULAR POWER SPECTRA

In this section we present the brightness temperature fluctuations of the redshifted 21-cm signal, emitted from the hyperfine transition between the excited triplet states and the singlet states of neutral hydrogen atoms. It is fine to neglect the finite line width of the emission on large scales. And the stimulated emission and absorption can be neglected at low redshift. The 21 cm brightness temperature T_b is [17]:

$$T_b(z, \vec{n}) = \frac{3}{32\pi} \frac{h_p^3 n_{HI} A_{10}}{k_B E_{21}} \left| \frac{d\lambda}{dz} \right|. \quad (14)$$

Here h_p is the Planck's constant, $A_{10} \approx 2.869 \times 10^{-15} \text{ s}^{-1}$ is the spontaneous emission coefficient, k_B is Boltzmann's constant, and $E_{21} = 5.88 \mu\text{eV}$ is the rest-frame energy of a 21 cm photon. \vec{n} is the unit vector along the line of sight, n_{HI} is the rest-frame number density of neutral hydrogen atoms, λ is an affine parameter for the light path. Since the distribution of HI is a good tracer of the large scale structures of our Universe, it is quite natural to expand equation (14) to its background level and perturbation level, as have been done in the analysis of the large scale structure.

If we first exclude the contribution from perturbations, $|dz/d\lambda| = (1+z)H(z)E_{21}$, then the background brightness temperature is

$$\bar{T}_b(z) = \frac{3(h_p c)^3 \bar{n}_{HI} A_{10}}{32\pi k_B E_{21}^2 (1+z)H(z)} = 0.188 K h \Omega_{HI}(z) \frac{(1+z)^2}{E(z)}. \quad (15)$$

Here $H(z)$ is the Hubble parameter, $E(z) = H(z)/H_0$, H_0 is the Hubble constant. $\Omega_{HI}(z)$ is the comoving mass density of HI in units of the current critical density. In this paper, we take Ω_{HI} to be constant.

When considering perturbations,

$$n_{HI}(z, \vec{n}) = \bar{n}_{HI}(z)(1 + \delta_n(z, \vec{n})) = \bar{n}_{HI}(\bar{\tau}_z + \delta\tau)(1 + \delta_n(z, \vec{n})) = \bar{n}_{HI}(\bar{\tau}_z)(1 + \frac{\dot{\bar{n}}_{HI}}{n_{HI}}\delta\tau + \delta_n), \quad (16)$$

$$\left| \frac{d\lambda}{dz} \right|(z, \vec{n}) = \frac{a(\bar{\tau}_z)}{\mathcal{H}(\bar{\tau}_z)E_{21}(1+z)} \left[1 - (\frac{\dot{\mathcal{H}}}{\mathcal{H}} - \mathcal{H})\delta\tau - \frac{1}{\mathcal{H}} \frac{d\Psi}{d\tau} + \frac{1}{\mathcal{H}}(\dot{\Phi} + \dot{\Psi}) + \frac{1}{\mathcal{H}}\vec{n} \cdot \frac{d\vec{v}}{d\eta} + \Psi + \vec{n} \cdot \vec{v} \right], \quad (17)$$

so the perturbation to the brightness temperature is

$$\Delta_{T_b}(z, \vec{n}) = \frac{\delta T_b(z, \vec{n})}{T_b(z)} = \delta_n + \frac{\dot{\bar{n}}_{HI}}{n_{HI}} \delta\tau - \left(\frac{\dot{\mathcal{H}}}{\mathcal{H}} - \mathcal{H} \right) \delta\tau - \frac{1}{\mathcal{H}} \frac{d\Psi}{d\tau} + \frac{1}{\mathcal{H}} (\dot{\Phi} + \dot{\Psi}) + \frac{1}{\mathcal{H}} \vec{n} \cdot \frac{d\vec{v}}{d\tau} + \vec{n} \cdot \vec{v} + \Psi. \quad (18)$$

The above equation is valid for all metric theories of gravity, including $f(R)$ gravity, one can refer to [17] for the details of the inferring process. Using the Euler equation (9) but in configuration space $\dot{\vec{v}} + \mathcal{H}\vec{v} + \nabla\Psi = 0$, it becomes

$$\Delta_{T_b}(z, \vec{n}) = \delta_n - \frac{1}{\mathcal{H}} \vec{n} \cdot [(\vec{n} \cdot \nabla) \vec{v}] + \left(\frac{d\ln(a^3 \bar{n}_{HI})}{d\tau} - \frac{\dot{\mathcal{H}}}{\mathcal{H}} - 2\mathcal{H} \right) \delta\tau + \frac{1}{\mathcal{H}} \dot{\Phi} + \Psi. \quad (19)$$

In this equation, the first term is the usual density term, and the second is the RSD term. The other term also have their physical meanings and origins, for example, the integrated Sachs-Wolfe (ISW) effect and Doppler shift. The first two terms are dominant over other terms [17, 28, 40], so here we just consider the matter density term and the RSD term in our later analysis. Since the distribution of HI gas follows that of the discrete sources in which the neutral gas reside in, there is some bias between the HI distribution and the underlying matter distribution. And we follow the assumption that the bias is scale-independent at the linear order. During the period of matter domination, the comoving gauge coincides with the synchronous gauge, then we have [17, 40]

$$\delta_n = b_{HI} \delta_m^{syn} + \left(\frac{d\ln(a^3 \bar{n}_{HI})}{d\tau} - 3\mathcal{H} \right) \frac{v_m}{k}, \quad (20)$$

where b_{HI} is the scale-independent bias, v_m is the Newtonian-gauge matter velocity and δ_m^{syn} is the matter overdensity in the synchronous gauge.

Due to the projection of the three dimensional HI distribution into the two dimensional sphere, for a fixed redshift, one can expand the brightness temperature in spherical harmonics, that is:

$$\Delta_{T_b}(z, \vec{n}) = \sum_{lm} \Delta_{T_b,lm}(z) Y_{lm}(\vec{n}). \quad (21)$$

Then express the perturbation coefficients $\Delta_{T_b,lm}(z)$ using the Fourier transforms of the perturbations, we have

$$\Delta_{T_b,lm}(z) = 4\pi i^l \int \frac{d^3 \vec{k}}{(2\pi)^{3/2}} \Delta_{T_b,l}(z, \vec{k}) Y_{lm}^*(\vec{k}). \quad (22)$$

Following equation (19), the l th multipole moment of Δ_{T_b} is

$$\Delta_{T_b,l}(z, \vec{k}) = \delta_n j_l(k\chi) + \frac{kv}{\mathcal{H}} j_l''(k\chi) + \left(\frac{1}{\mathcal{H}} \dot{\Phi} + \Psi \right) j_l(k\chi) - \left(\frac{1}{\mathcal{H}} \frac{d\ln(a^3 \bar{n}_{HI})}{d\tau} - \frac{\dot{\mathcal{H}}}{\mathcal{H}^2} - 2 \right) \left[\Psi j_l(k\chi) + v j_l'(k\chi) + \int_0^\chi (\dot{\Psi} + \dot{\Phi}) j_l(k\chi') d\chi' \right]. \quad (23)$$

where χ is the comoving distance to redshift z , $j_l(k\chi)$ is the spherical Bessel Function. The prime in $j_l'(k\chi)$, $j_l''(k\chi)$ is the derivative with respect to $k\chi$. We then integrate over a redshift (frequency) normalized window function centered at redshift z

$$W(z) = \begin{cases} 1/\Delta z, & (z - \Delta z/2 \leq z \leq z + \Delta z/2) \\ 0, & \text{otherwise} \end{cases} \quad (24)$$

to get

$$\Delta_{T_b,l}^W(\vec{k}) = \int_0^\infty dz W(z) \Delta_{T_b,l}(z, \vec{k}). \quad (25)$$

Then the angular power spectrum between redshift windows is

$$C_l^{WW'} = 4\pi \int dk \mathcal{P}_{\mathcal{R}}(k) \Delta_{T_b,l}^W(k) \Delta_{T_b,l}^{W'}(k). \quad (26)$$

Here $\mathcal{P}_{\mathcal{R}}(k)$ is the dimensionless power spectrum of the primordial curvature perturbation \mathcal{R} , and we define $\Delta_{T_b,l}^W(k) \equiv \Delta_{T_b,l}^W(\vec{k})/\mathcal{P}_{\mathcal{R}}(\vec{k})$.

In Figure 1, we plot the auto-spectra for $f(R)$ gravity at redshift $z = 0.27$ with the channel bandwidth being 9.33MHz, with just the first two terms in equation (19). In the top panel, we plot the auto-spectra for $f(R)$ gravity at $B_0 = 0, 0.01, 0.1, 1, 3, 4$. $B_0 = 0$ is regarded as the base case, which is the same as Λ CDM. One can see that as the B_0 becomes larger, the auto-spectra become larger, too. In the bottom panel, we plot the deflections of auto-spectra for $f(R)$ gravity with respect to Λ CDM. Similarly, the B_0 is larger, the differences of auto-spectra between $f(R)$ gravity and Λ CDM are greater.

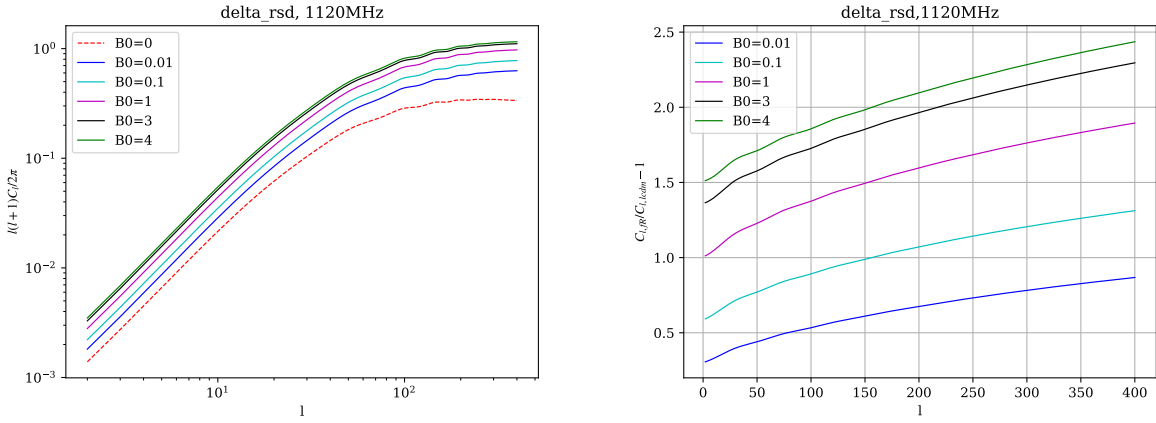


FIG. 1: Angular power spectra of the HI 21 cm signal at redshift $z = 0.27$ with a channel bandwidth of 9.33 MHz. Left panel: auto-spectra for different values of the $f(R)$ parameter B_0 , where $B_0 = 0$ corresponds to the Λ CDM case. Right panel: fractional deviations of the $f(R)$ spectra relative to Λ CDM. Larger values of B_0 lead to stronger departures from Λ CDM, especially on small angular scales.

IV. NOISES AND THE FISHER MATRIX

To have a forecast for the constraints of the cosmological parameters from the upcoming 21cm IM experiments, we need not only the angular power spectrum from the HI 21cm signal, but also that from the noise. In our analysis, we assume the BINGO and SKA surveys as representative IM experiments.

A. surveys

BINGO is a single-dish, drift-scan radio telescope currently under construction in the northeast of Brazil, conceived as a pathfinder for low-redshift 21 cm intensity mapping and the first-generation radio detection of BAO [22]. The baseline Phase 1 concept employs a dual-reflector optical system with two ~ 40 m-class dishes in a crossed-Dragone configuration, illuminating a focal plane populated by 28 feed horns [24]. Each horn is coupled to a receiver chain providing dual-polarization measurements, often implemented as two circular polarizations.

BINGO is designed to operate in the frequency interval $980 \text{ MHz} \leq \nu \leq 1260 \text{ MHz}$, which corresponds to the 21 cm rest frequency $\nu_{21} = 1420 \text{ MHz}$ mapped into the redshift range $0.127 \lesssim z \lesssim 0.449$, thereby targeting the low-redshift regime where BAO measurements place strong leverage on late-time cosmology and dark-sector phenomenology [22, 28]. The survey strategy is optimized to minimize instrumental complexity and time-variable systematics by adopting a transit mode with no moving dishes [23]. With the primary mirror pointing at approximately $\delta \simeq -15^\circ$, BINGO scans an instantaneous declination strip of about 14.75° and is designed to cover $\sim 13\%$ of the sky over nominal operation [23]. To avoid nonlinear effects, we assume the channel bandwidth to be 10 MHz. BINGO has an angular resolution of $\theta_{FWHM} = 40$ arcmin, with the full-width half-maximum (FWHM) beam resolution θ_{FWHM} defined by $\theta_{FWHM} = 1.2\lambda_{med}/D_{dish}$, where $D_{dish} = 34\text{m}$ is the illuminated aperture, and $\lambda_{med} = c/\nu_{med}$ is the wavelength at the medium frequency ν_{med} of the entire range [22–24]. And $\theta_{FWHM} = 40$ arcmin corresponds to the angular resolution of BINGO at 1 GHz.

The SKA is an international effort to construct a next-generation radio observatory, which will ultimately achieve a total collecting area of order one square kilometre, providing unprecedented sensitivity for cosmological and astrophysical studies [31]. The SKA will be implemented in two major phases, referred to as SKA1 and SKA2. While SKA1 is currently under construction, the detailed configuration of SKA2 has not yet been finalized and will be defined at a later stage. Phase 1 of the project consists of two complementary instruments: SKA1-MID and SKA1-LOW. SKA1-MID is a dish-based array located in the Northern Cape province of South Africa, whereas SKA1-LOW is a low-frequency aperture array situated near Geraldton in Western Australia [31]. SKA1-MID operates over the frequency range 350–1750 MHz, while SKA1-LOW covers 50–350 MHz, allowing the SKA to probe large-scale structure over a wide range of redshifts using the redshifted 21 cm line. In this work, we focus on SKA1-MID, as its frequency coverage corresponds to the redshift range $z \lesssim 3$, which is particularly relevant for studies of late-time cosmology and the dark sector [41].

The SKA1-MID instrument will operate primarily in two frequency bands of cosmological interest. Band 1 covers the frequency interval 350–1050 MHz, corresponding to a redshift range $0.35 < z < 3.06$, while Band 2 spans 950–1750 MHz, probing the low-redshift Universe over $0 < z < 0.49$ via the 21 cm emission line [31]. SKA1-MID is a dish array composed of multiple sub-arrays, including the 64 dishes of the MeerKAT precursor instrument, each with a diameter of 13.5 m, and 133 newly built SKA1 dishes with diameters of 15 m. Following the treatment adopted in [41], we assume that all 197 dishes can be approximated as having a uniform diameter of 15 m and are equipped with dual-polarization receivers, an assumption that does not significantly affect the resulting cosmological forecasts. The beam full-width at half-maximum is evaluated at the median frequency of each band. For Band 1, the angular resolution is $\theta_{FWHM} = 1.96^\circ$ at a median frequency $\nu_{\text{med}} = 700$ MHz, while for Band 2 it is $\theta_{FWHM} = 1.17^\circ$ at $\nu_{\text{med}} = 1177.5$ MHz [41]. For consistency and to facilitate a direct comparison with the BINGO experiment, we adopt a frequency channel width of 10 MHz for both SKA1-MID bands throughout this work.

Following [31], we can calculate the system temperature of SKA1-MID array through

$$T_{\text{sys}} = T_{rx} + T_{spl} + T_{CMB} + T_{gal}, \quad (27)$$

where $T_{spl} \approx 3$ K contributes from ‘spill-over’, and the CMB temperature is $T_{CMB} \approx 2.73$ K. T_{gal} contributes from our own galaxy as a function of frequency, as given by

$$T_{gal} = 25\text{K}(408\text{MHz}/\nu)^{2.75}. \quad (28)$$

T_{rx} is the receiver noise temperature, for Band 1, $T_{rx} = 15\text{K} + 30(\frac{\nu}{\text{GHz}} - 0.75)^2$; for Band 2, $T_{rx} = 7.5$ K. For Band 2, we can assume a constant Galactic contribution of $T_{gal} \approx 1.3$ K, since at high frequencies of the operation frequency range of Band 2, it is subdominant. So, the system temperature for Band 2 is constant, $T_{sys} = 15$ K. And the system temperature for BINGO is also a constant, 70 K. The sky coverage for SKA1-MID Band 1 and Band 2 are assumed to be 20000 and 5000 deg² respectively, and assuming one year operation time. Details of the configurations of BINGO and SKA1-MID are summarized in Table I.

	Bingo	SKA Band 1	SKA Band 2
redshift range	[0.13,0.45]	[0.36,3]	[0.01,0.49]
frequency range(MHz)	[980,1260]	[350,1050]	[950,1410]
Number of dishes	1	197	197
Number of beams (dual pol.)	28×2	1×2	1×2
Number of channels	28	70	46
Channel bandwidth ($\delta\nu$, MHz)	10	10	10
Resolution (θ_{FWHM} , arcmin)	40	106	63
System temperature (T_{sys} , K)	70	Eq. (27)	15
Survey time (t_{obs} , yr)	1	1	1
Sky coverage (Ω_{sur} , deg ²)	3000	20000	5000

TABLE I: Survey specifications adopted in this work for BINGO and SKA1-MID (Band 1 and Band 2). These parameters are used to compute the instrumental noise and forecast the cosmological constraints.

B. noises

In this work we include the thermal noise and the shot noise. The thermal noise is from the voltages generated by thermal agitations in the resistive components of the receiver. Then, the pixel noise is given by

$$\sigma_T = \frac{T_{sys}}{\sqrt{t_{pix}\delta\nu}}, \quad (29)$$

where $\delta\nu$ is the channel bandwidth, T_{sys} is the total system temperature, t_{pix} is the integration time per pixel, obtained from

$$t_{pix} = t_{obs} \frac{n_{beam} n_d \Omega_{pix}}{\Omega_{sur}}. \quad (30)$$

Where t_{obs} is the operation time of one year of the survey, n_{beam} and n_d is the number of beams and dishes, respectively. $\Omega_{pix} \propto \theta_{FWHM}^2$ is the sky area per pixel, and Ω_{sur} is the total sky area of the survey. Then the angular power spectrum of thermal noise is

$$N_l(z_i, z_j) = \frac{4\pi}{N_{pix}} \sigma_{T,i} \sigma_{T,j}. \quad (31)$$

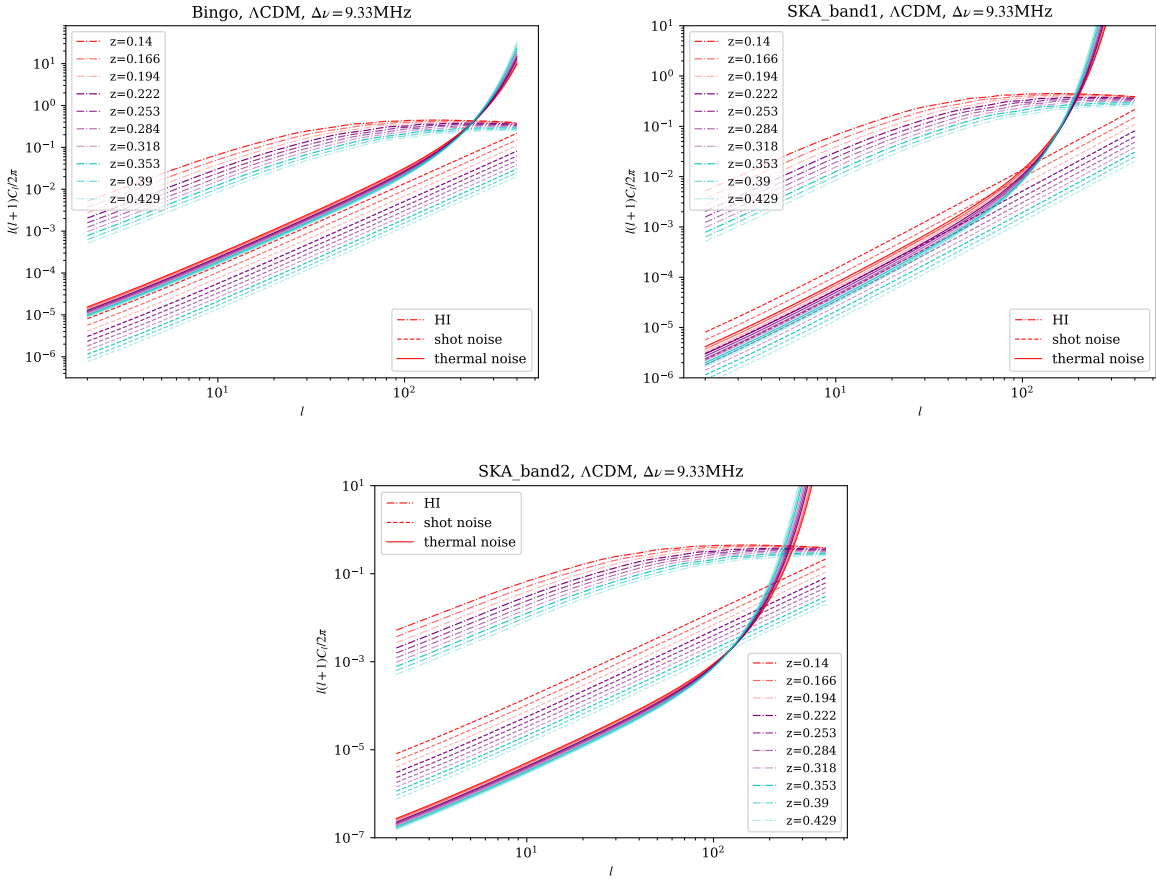


FIG. 2: Angular power spectra of the HI 21 cm signal, thermal noise, and shot noise for BINGO (top left), SKA1-MID Band 1 (top right), and Band 2 (bottom), evaluated at multiple redshift bins. The HI signal dominates over instrumental noise on large angular scales. The thermal noise contribution is smallest for SKA Band 2.

where N_{pix} is the number of pixels in the map, $\sigma_{T,i}, \sigma_{T,j}$ are that in the equation (29) at different redshift. Here, we assume $N_l(z_i, z_j) = 0$ if $z_i \neq z_j$.

Equation (31) is for a perfect beam receiver measuring, when considering the beam resolution θ_{FWHM} , there is beam corrections to the angular power spectrum of the thermal noise, reducing the signal by a factor of b_l^2 [41],

$$b_l(z_i) = \exp\left(-\frac{1}{2}l^2\sigma_{b,i}^2\right), \quad (32)$$

where $\sigma_{b,i} = \theta_B(z_i)/\sqrt{8\ln 2}$ [42] and $\theta_B(z_i) = \theta_{FWHM}(\nu_{med})\nu_{med}/\nu_i$.

The thermal noise is from the instrument, while the shot noise is actually a part of the signal itself. Since the HI sources are discrete, it will contribute to the auto-spectra measured in the signal, behave as $C_l^{shot} = \bar{T}_b^2(z)/\bar{N}(z)$ [17]. Recall that $\bar{T}_b(z)$ is the average brightness temperature of the 21cm emission line, and $\bar{N}(z)$ is the angular density of the sources. $\bar{N}(z)$ is given by

$$\bar{N}(z) = \frac{n_0 c}{H_0} \int \frac{\chi^2(z)}{E(z)} dz, \quad (33)$$

where $n_0 = 0.03h^3 \text{Mpc}^{-3}$ [43] is the comoving number density of sources.

In Figure 2, we plot the auto-spectra for the HI signal, the thermal noise and shot noise. The top left panel shows the plot for BINGO at ten different redshifts, with the channel bandwidth being 9.33MHz. It shows that the auto-spectra for HI signal is larger than that of the thermal noise, and the shot noise is the smallest. For all of the three kinds of auto-spectra, as the redshift goes higher, the auto-spectra becomes smaller. The top right and bottom panels show the plots for SKA1-MID Band 1 and 2, respectively. Since the HI signal and shot noise auto-spectra are

identical across BINGO, SKA1-MID Band 1, and SKA1-MID Band 2, the thermal noise auto-spectra can be directly compared: SKA1-MID Band 2 exhibits the lowest amplitude, followed by SKA1-MID Band 1, while BINGO yields the highest thermal noise auto-spectrum.

C. Fisher matrix

We use Fisher matrix to estimate the uncertainty of the parameters from the IM data. For a set of cosmological parameters

$$\boldsymbol{\theta} = \{\Omega_b h^2, \Omega_c h^2, \log(10^{10} A_s), n_s, h, B_0, b_{HI}\}, \quad (34)$$

the Fisher matrix for the parameters θ_i is defined as the ensemble average of the Hessian matrix of the log-likelihood function [44]

$$F_{ij} = \left\langle -\frac{\partial \ln \mathcal{L}}{\partial \theta_i \partial \theta_j} \right\rangle = \frac{1}{2} \text{Tr} \left[\mathbf{C}^{-1} \frac{\partial \mathbf{C}}{\partial \theta_i} \mathbf{C}^{-1} \frac{\partial \mathbf{C}}{\partial \theta_j} \right]. \quad (35)$$

Here the covariance matrix \mathbf{C} is given by

$$\mathbf{C} = \begin{bmatrix} A_{l=2} & 0 & \dots & 0 \\ 0 & A_3 & \dots & 0 \\ \vdots & \vdots & \dots & \vdots \\ 0 & 0 & \dots & A_n \end{bmatrix}, \quad (36)$$

where

$$A_l = (2l + 1) \begin{bmatrix} C_l(z_1, z_1) & C_l(z_1, z_2) & \dots & C_l(z_1, z_n) \\ C_l(z_2, z_1) & C_l(z_2, z_2) & \dots & C_l(z_2, z_n) \\ \vdots & \vdots & \dots & \vdots \\ C_l(z_n, z_1) & C_l(z_n, z_2) & \dots & C_l(z_n, z_n) \end{bmatrix} \quad (37)$$

and

$$C_l(z_i, z_j) = C_l^{HI}(z_i, z_j) + \delta_{ij} C_l^{shot}(z_i, z_j) + N_l(z_i, z_j) B_l(z_i, z_j). \quad (38)$$

V. RESULTS

In this section, we present Fisher matrix forecasts for constraining cosmological parameters and the $f(R)$ gravity parameter B_0 using upcoming HI 21 cm IM surveys. We consider three experimental configurations, BINGO, SKA1-MID Band 1, and SKA1-MID Band 2. And we further quantify the gain in constraining power achieved by combining each IM survey with Planck CMB priors. The marginalized 1σ uncertainties on all parameters are summarized in Table II, and the key parameter degeneracies are illustrated in Figs. 3 and 4.

We forecast the marginalized constraints on the parameters $\boldsymbol{\theta} = \{\Omega_b h^2, \Omega_c h^2, \ln(10^{10} A_s), n_s, h, B_0, b_{HI}\}$, around a fiducial Λ CDM background with $B_0 = 0$ (see Table II for the fiducial values). As expected, BINGO alone yields relatively weak constraints on the standard cosmological parameters, primarily due to its limited sky coverage and narrow redshift range. Remarkably, however, even this pathfinder IM experiment exhibits measurable sensitivity late-time modifications of gravity, yielding $\sigma(B_0) \simeq 2.27 \times 10^{-6}$. This result confirms that low-redshift 21 cm IM surveys can probe $f(R)$ gravity not only via background evolution but, more robustly, through its distinct imprint on the growth of cosmic structure. SKA1-MID shows substantially stronger constraining power. With its larger sky coverage, broader redshift range and lower instrumental noise, both Band 1 and Band 2 of SKA1-MID reduce the marginalized 1σ uncertainties on $(\Omega_b h^2, \Omega_c h^2, A_s, n_s, h)$ by approximately an order of magnitude relative to BINGO. In particular, SKA Band 2 achieves $\sigma(h) \simeq 1.88 \times 10^{-3}$, $\sigma(B_0) \simeq 6.37 \times 10^{-8}$, highlighting its excellent sensitivity to scale-dependent growth signatures induced by modified gravity at low redshift. When Planck priors are included, the constraints on the parameters $(\Omega_b h^2, \Omega_c h^2, A_s, n_s, h)$ tighten significantly for all IM surveys, demonstrating the powerful complementarity between early-universe CMB probes and late-time large-scale structure measurements. Importantly, IM data also break key degeneracies affecting B_0 , leading to a marked improvement in its determination

over Planck alone. For example, combining BINGO with Planck yields $\sigma(B_0) \simeq 1.09 \times 10^{-6}$, while the SKA Band 2 and Planck combination achieves the strongest constraint to date, $\sigma(B_0) \simeq 3.75 \times 10^{-8}$.

Figure 3 shows the marginalized two-dimensional confidence contours (68% and 95%). For IM-only forecasts, strong degeneracies appear between B_0 and late-time parameters that affect the amplitude and evolution of clustering, especially the Hubble parameter h and the HI bias b_{HI} . This is expected because modified gravity can partially mimic changes in the late-time expansion rate and growth history. These degeneracies are efficiently reduced once Planck priors are included, since CMB data strongly constrain the early-Universe background cosmology and primordial parameters. The joint IM+Planck constraints therefore isolate the late-time, scale-dependent signatures characteristic of $f(R)$ gravity, leading to significantly smaller confidence regions.

The degeneracy between B_0 and h is shown explicitly in Fig. 4, where we plot the 68% and 95% confidence contours for BINGO, SKA Band 1, and SKA Band 2, both alone and in combination with Planck. For IM-only surveys, the contours are elongated in the B_0 - h plane, indicating a strong degeneracy between these two parameters, with the effect being most pronounced for BINGO and reduced for SKA configurations due to their improved sensitivity. After adding Planck priors, the contours shrink substantially and become much tighter in h , showing that the uncertainty in the expansion history no longer dominates the determination of B_0 . Among all combinations, SKA Band 2 + Planck provides the tightest constraints, consistent with the smallest $\sigma(B_0)$ reported in Table II.

Figure 5 shows the ratio of the marginalized uncertainties of cosmological parameters obtained by truncating the angular power spectrum at a given maximum multipole ℓ_{max} to those obtained with $\ell_{\text{max}} = 400$, i.e. $\sigma(\theta_i; \ell_{\text{max}})/\sigma(\theta_i; \ell_{\text{max}} = 400)$, as a function of ℓ_{max} . This definition of the vertical axis follows that adopted in Fig. 11 of Ref. [40], allowing a direct assessment of how the parameter constraints converge as smaller angular scales are progressively included. For all survey configurations, the ratios decrease rapidly with increasing ℓ_{max} and approach unity at $\ell_{\text{max}} \simeq 300$ –400, indicating that the constraints on most parameters are already close to saturation once multipoles up to a few hundred are included. This behavior demonstrates that the dominant Fisher information is carried by large- and intermediate-scale modes, while the contribution from very high multipoles is subdominant. For clarity, Fig. 5 is plotted using a dual y -axis, where parameters with significantly different amplitudes of $\sigma(\theta_i)/\sigma(\theta_i; \ell_{\text{max}} = 400)$ are separated onto the left and right axes. This presentation highlights the relative convergence rates of different parameters without affecting the physical interpretation. In particular, late-time parameters such as B_0 and b_{HI} exhibit a slower convergence with ℓ_{max} than background parameters, reflecting their stronger sensitivity to large-scale modes. This explains why the constraints on B_0 are primarily driven by low- ℓ information, consistent with the results shown in Figs. 3 and 4.

	$\Omega_b h^2$	$\Omega_c h^2$	$\ln(10^{10} A_s)$	n_s	h	B_0	b_{HI}
Fiducial values	0.022383	0.12011	3.044	0.96605	0.6732	0.00	1.00
Bingo	1.77×10^{-2}	6.31×10^{-2}	9.11×10^{-1}	1.45×10^{-1}	1.68×10^{-1}	2.27×10^{-6}	4.64×10^{-2}
SKA_Band1	1.09×10^{-3}	4.44×10^{-3}	6.63×10^{-2}	1.83×10^{-2}	1.13×10^{-2}	4.48×10^{-6}	7.69×10^{-3}
SKA_Band2	9.33×10^{-4}	2.33×10^{-3}	4.77×10^{-2}	1.13×10^{-2}	1.88×10^{-3}	6.37×10^{-8}	2.12×10^{-2}
Planck	1.53×10^{-4}	1.23×10^{-3}	2.16×10^{-2}	4.24×10^{-3}	5.87×10^{-3}	5.31×10^{-2}	-
Bingo+Planck	1.40×10^{-4}	1.01×10^{-3}	1.98×10^{-2}	3.89×10^{-3}	4.75×10^{-3}	1.09×10^{-6}	1.49×10^{-2}
SKA_Band1+Planck	1.16×10^{-4}	4.85×10^{-4}	1.30×10^{-2}	3.12×10^{-3}	2.06×10^{-3}	3.89×10^{-6}	6.70×10^{-3}
SKA_Band2+Planck	1.08×10^{-4}	4.57×10^{-4}	1.76×10^{-2}	2.77×10^{-3}	1.69×10^{-3}	3.75×10^{-8}	1.02×10^{-2}

TABLE II: Marginalized 1σ uncertainties on cosmological parameters and the $f(R)$ gravity parameter B_0 obtained from Fisher-matrix forecasts. Results are shown for BINGO, SKA1-MID Band 1, and Band 2, both alone and in combination with Planck CMB priors.

VI. CONCLUSION

In this work, we have investigated the potential of future HI 21 cm intensity mapping surveys to constrain $f(R)$ gravity, focusing on the Compton wavelength parameter B_0 . Using the Fisher matrix formalism, we forecast constraints from BINGO and SKA1-MID (Band 1 and Band 2), both alone and in combination with Planck CMB priors.

We find that low-redshift 21 cm IM surveys provide a powerful probe of modified gravity through their sensitivity to the growth of large-scale structure. Even BINGO alone is able to place meaningful constraints on B_0 , while SKA1-MID significantly improves the precision due to its larger sky coverage and lower instrumental noise. Among the considered configurations, SKA Band 2 yields the tightest constraints, highlighting its strong sensitivity to scale-dependent growth effects induced by $f(R)$ gravity.

We further demonstrate that combining 21 cm IM data with Planck priors leads to substantial improvements in the constraints on B_0 . The CMB data efficiently break degeneracies with background cosmological parameters, allowing

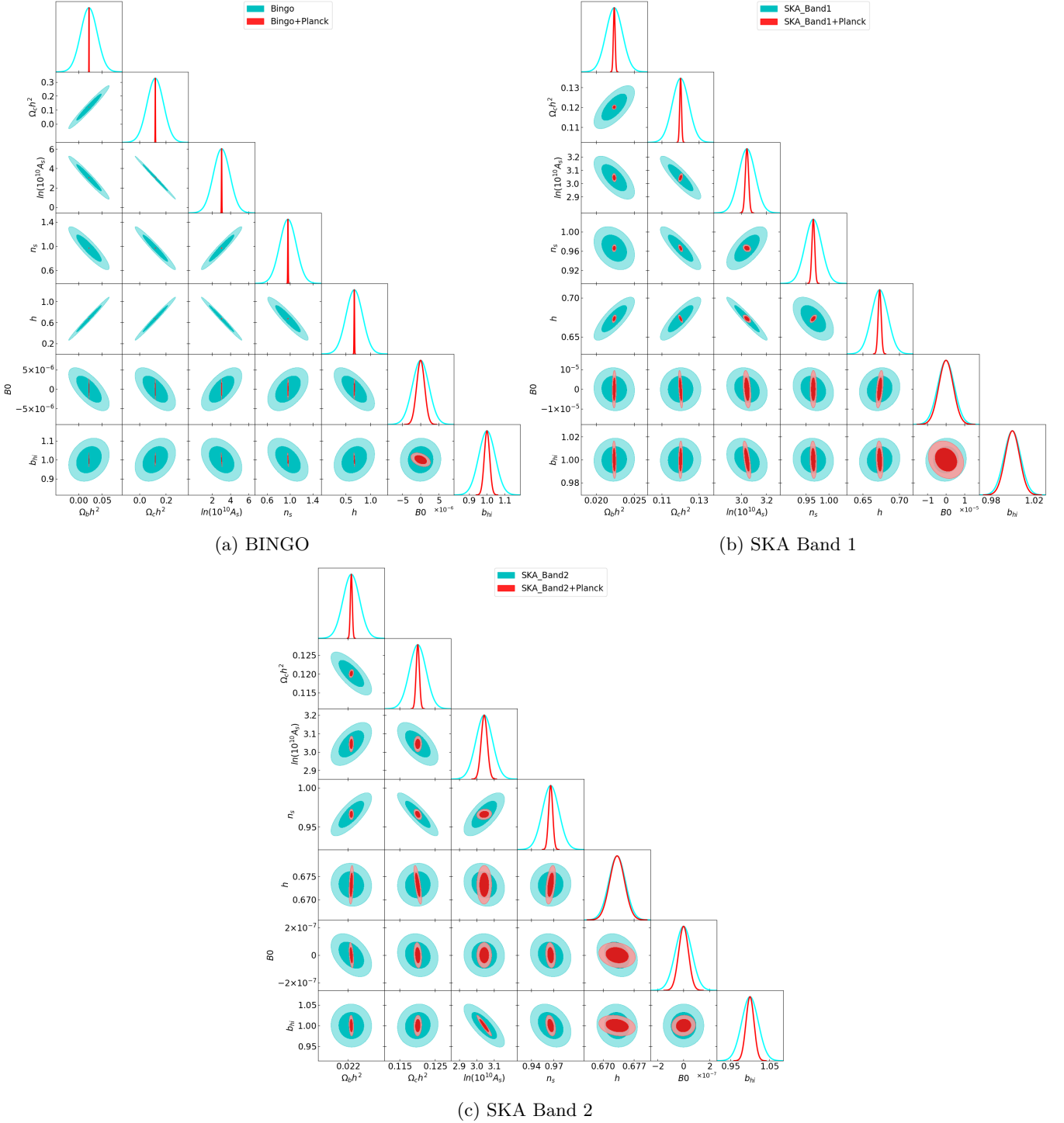


FIG. 3: Marginalized one- and two-dimensional confidence regions (68% and 95%) for selected cosmological parameters and the $f(R)$ gravity parameter B_0 . Results are shown for BINGO (top left), SKA1-MID Band 1 (top right), and Band 2 (bottom), both with and without Planck CMB priors. The inclusion of Planck data significantly reduces parameter degeneracies and tightens the constraints.

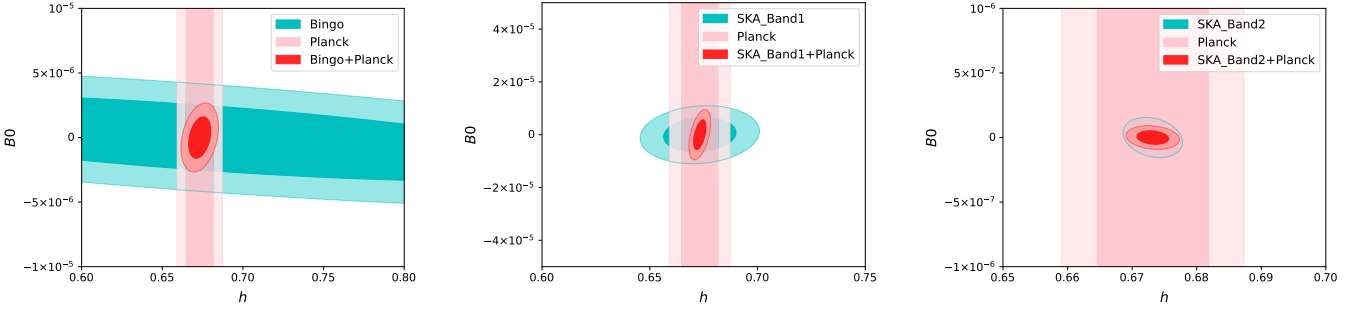


FIG. 4: Marginalized 68% and 95% confidence contours in the B_0 - h plane for BINGO (left), SKA1-MID Band 1 (middle), and Band 2 (right). Results are shown for IM-only forecasts and in combination with Planck priors. The strong degeneracy between B_0 and h present in IM-only surveys is efficiently broken when CMB information is included.

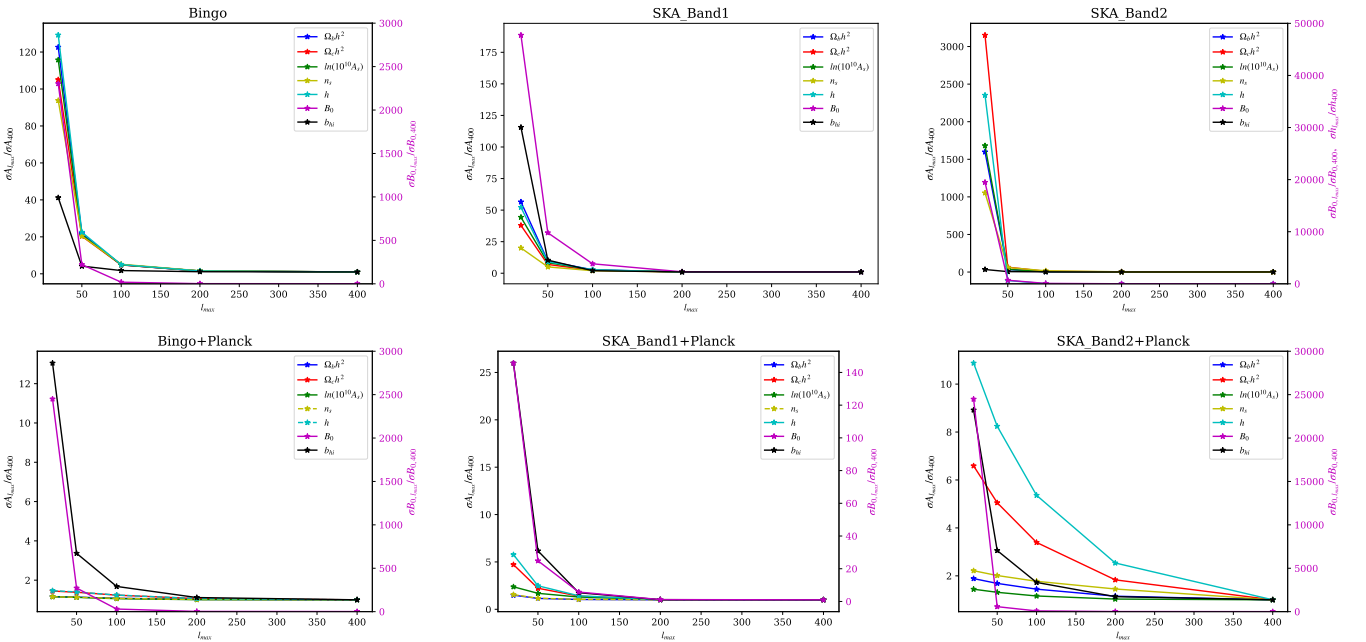


FIG. 5: Ratios of the marginalized parameter uncertainties obtained with a maximum multipole ℓ_{\max} to those obtained with $\ell_{\max} = 400$, as functions of ℓ_{\max} . Results are shown for different survey configurations. A dual y -axis is adopted to display parameters with different amplitudes of $\sigma(\theta_i)/\sigma(\theta_i; \ell_{\max} = 400)$. The figure illustrates the convergence of parameter constraints as smaller angular scales are progressively included, showing that most constraints saturate at $\ell_{\max} \sim 300$ -400.

the late-time information from 21 cm observations to isolate signatures of modified gravity. Our analysis shows that the dominant contribution to constraining B_0 arises from large-scale modes, consistent with the scale dependence of $f(R)$ effects.

Overall, our results indicate that upcoming HI intensity mapping experiments, especially SKA1-MID, will play a crucial role in testing deviations from General Relativity on cosmological scales. When combined with CMB observations, these surveys offer a promising avenue for placing stringent constraints on $f(R)$ gravity and probing the nature of cosmic acceleration. In future work, it will be important to incorporate a more realistic treatment of foreground contamination, instrumental systematics, and nonlinear effects, in order to fully assess the robustness of these constraints in practical observational scenarios.

ACKNOWLEDGMENTS

We thank Chang Feng for useful discussions. This work is supported by National Natural Science Fund of China under Grants Nos. 12175192, and Yangzhou Science and Technology Planning Project in Jiangsu Province of China (YZ2025233).

-
- [1] S. Perlmutter *et al.* (Supernova Cosmology Project), “Measurements of Ω and Λ from 42 High Redshift Supernovae,” *Astrophys. J.* **517**, 565–586 (1999), [arXiv:astro-ph/9812133](https://arxiv.org/abs/astro-ph/9812133).
- [2] Adam G. Riess *et al.*, “A Comprehensive Measurement of the Local Value of the Hubble Constant with $1 \text{ km s}^{-1} \text{ Mpc}^{-1}$ Uncertainty from the Hubble Space Telescope and the SH0ES Team,” *Astrophys. J. Lett.* **934**, L7 (2022), [arXiv:2112.04510](https://arxiv.org/abs/2112.04510) [astro-ph.CO].
- [3] N. Aghanim *et al.* (Planck), “Planck 2018 results. VI. Cosmological parameters,” *Astron. Astrophys.* **641**, A6 (2020), [Erratum: *Astron. Astrophys.* 652, C4 (2021)], [arXiv:1807.06209](https://arxiv.org/abs/1807.06209) [astro-ph.CO].
- [4] Marika Asgari *et al.* (KiDS), “KiDS-1000 Cosmology: Cosmic shear constraints and comparison between two point statistics,” *Astron. Astrophys.* **645**, A104 (2021), [arXiv:2007.15633](https://arxiv.org/abs/2007.15633) [astro-ph.CO].
- [5] C. Doux *et al.* (DES), “Dark energy survey year 3 results: cosmological constraints from the analysis of cosmic shear in harmonic space,” *Mon. Not. Roy. Astron. Soc.* **515**, 1942–1972 (2022), [arXiv:2203.07128](https://arxiv.org/abs/2203.07128) [astro-ph.CO].
- [6] Alexei A. Starobinsky, “A New Type of Isotropic Cosmological Models Without Singularity,” *Phys. Lett. B* **91**, 99–102 (1980).
- [7] Antonio De Felice and Shinji Tsujikawa, “ $f(R)$ theories,” *Living Rev. Rel.* **13**, 3 (2010), [arXiv:1002.4928](https://arxiv.org/abs/1002.4928) [gr-qc].
- [8] Taishi Katsuragawa and Shinya Matsuzaki, “Cosmic History of Chameleonic Dark Matter in $F(R)$ Gravity,” *Phys. Rev. D* **97**, 064037 (2018), [Erratum: *Phys. Rev. D* 97, 129902 (2018)], [arXiv:1708.08702](https://arxiv.org/abs/1708.08702) [gr-qc].
- [9] Thomas P. Sotiriou and Valerio Faraoni, “ $f(R)$ Theories Of Gravity,” *Rev. Mod. Phys.* **82**, 451–497 (2010), [arXiv:0805.1726](https://arxiv.org/abs/0805.1726) [gr-qc].
- [10] Shin’ichi Nojiri and Sergei D. Odintsov, “Introduction to modified gravity and gravitational alternative for dark energy,” *eConf* **C0602061**, 06 (2006), [arXiv:hep-th/0601213](https://arxiv.org/abs/hep-th/0601213).
- [11] Bin Hu, Michele Liguori, Nicola Bartolo, and Sabino Matarrese, “Parametrized modified gravity constraints after Planck,” *Phys. Rev. D* **88**, 123514 (2013), [arXiv:1307.5276](https://arxiv.org/abs/1307.5276) [astro-ph.CO].
- [12] Lucas Lombriser, Anze Slosar, Uros Seljak, and Wayne Hu, “Constraints on $f(R)$ gravity from probing the large-scale structure,” *Phys. Rev. D* **85**, 124038 (2012), [arXiv:1003.3009](https://arxiv.org/abs/1003.3009) [astro-ph.CO].
- [13] Richard A. Battye, Boris Bolliet, and Francesco Pace, “Do cosmological data rule out $f(\mathcal{R})$ with $w \neq -1$?” *Phys. Rev. D* **97**, 104070 (2018), [arXiv:1712.05976](https://arxiv.org/abs/1712.05976) [astro-ph.CO].
- [14] Jason Dossett, Bin Hu, and David Parkinson, “Constraining models of $f(R)$ gravity with Planck and WiggleZ power spectrum data,” *JCAP* **03**, 046 (2014), [arXiv:1401.3980](https://arxiv.org/abs/1401.3980) [astro-ph.CO].
- [15] Matteo Cataneo, David Rapetti, Fabian Schmidt, Adam B. Mantz, Steven W. Allen, Douglas E. Applegate, Patrick L. Kelly, Anja von der Linden, and R. Glenn Morris, “New constraints on $f(R)$ gravity from clusters of galaxies,” *Phys. Rev. D* **92**, 044009 (2015), [arXiv:1412.0133](https://arxiv.org/abs/1412.0133) [astro-ph.CO].
- [16] Yun-He Li, Jing-Fei Zhang, and Xin Zhang, “Probing $f(R)$ cosmology with sterile neutrinos via measurements of scale-dependent growth rate of structure,” *Phys. Lett. B* **744**, 213–217 (2015), [arXiv:1502.01136](https://arxiv.org/abs/1502.01136) [astro-ph.CO].
- [17] Alex Hall, Camille Bonvin, and Anthony Challinor, “Testing General Relativity with 21-cm intensity mapping,” *Phys. Rev. D* **87**, 064026 (2013), [arXiv:1212.0728](https://arxiv.org/abs/1212.0728) [astro-ph.CO].
- [18] Richard A. Battye, Rod D. Davies, and Jochen Weller, “Neutral hydrogen surveys for high redshift galaxy clusters and proto-clusters,” *Mon. Not. Roy. Astron. Soc.* **355**, 1339–1347 (2004), [arXiv:astro-ph/0401340](https://arxiv.org/abs/astro-ph/0401340).
- [19] Piero Madau, Avery Meiksin, and Martin J. Rees, “21-CM tomography of the intergalactic medium at high redshift,” *Astrophys. J.* **475**, 429 (1997), [arXiv:astro-ph/9608010](https://arxiv.org/abs/astro-ph/9608010).
- [20] Steven R. Furlanetto, “The 21-cm Line as a Probe of Reionization,” (2015), [arXiv:1511.01131](https://arxiv.org/abs/1511.01131) [astro-ph.CO].
- [21] Jordan Mirocha, “Astrophysics from the 21-cm background,” (2019), [arXiv:1909.12595](https://arxiv.org/abs/1909.12595) [astro-ph.CO].
- [22] Elcio Abdalla *et al.*, “The BINGO project - I. Baryon acoustic oscillations from integrated neutral gas observations,” *Astron. Astrophys.* **664**, A14 (2022), [arXiv:2107.01633](https://arxiv.org/abs/2107.01633) [astro-ph.CO].
- [23] Carlos A. Wuensche *et al.*, “The BINGO project - II. Instrument description,” *Astron. Astrophys.* **664**, A15 (2022), [arXiv:2107.01634](https://arxiv.org/abs/2107.01634) [astro-ph.IM].
- [24] Filipe B. Abdalla *et al.*, “The BINGO Project - III. Optical design and optimization of the focal plane,” *Astron. Astrophys.* **664**, A16 (2022), [arXiv:2107.01635](https://arxiv.org/abs/2107.01635) [astro-ph.IM].
- [25] Vincenzo Liccardo *et al.*, “The BINGO project - IV. Simulations for mission performance assessment and preliminary component separation steps,” *Astron. Astrophys.* **664**, A17 (2022), [arXiv:2107.01636](https://arxiv.org/abs/2107.01636) [astro-ph.CO].
- [26] Karin S. F. Fornazier *et al.*, “The BINGO project - V. Further steps in component separation and bispectrum analysis,” *Astron. Astrophys.* **664**, A18 (2022), [arXiv:2107.01637](https://arxiv.org/abs/2107.01637) [astro-ph.CO].
- [27] Jiajun Zhang *et al.*, “The BINGO project - VI. HI halo occupation distribution and mock building,” *Astron. Astrophys.* **664**, A19 (2022), [arXiv:2107.01638](https://arxiv.org/abs/2107.01638) [astro-ph.CO].
- [28] Andre A. Costa *et al.*, “The BINGO project - VII. Cosmological forecasts from 21 cm intensity mapping,” *Astron. Astro-*

- phys. **664**, A20 (2022), arXiv:2107.01639 [astro-ph.CO].
- [29] Marcelo V. dos Santos *et al.*, “The BINGO Project - IX. Search for fast radio bursts – A forecast for the BINGO interferometry system,” *Astron. Astrophys.* **681**, A120 (2024), arXiv:2308.06805 [astro-ph.IM].
- [30] Xue Zhang *et al.*, “The BINGO/ABDUS Project: Forecast for Cosmological Parameters from a Mock Fast Radio Burst Survey,” *Astrophys. J.* **991**, 189 (2025), arXiv:2411.17516 [astro-ph.CO].
- [31] David J. Bacon *et al.* (SKA), “Cosmology with Phase 1 of the Square Kilometre Array: Red Book 2018: Technical specifications and performance forecasts,” *Publ. Astron. Soc. Austral.* **37**, e007 (2020), arXiv:1811.02743 [astro-ph.CO].
- [32] Yong-Seon Song, Wayne Hu, and Ignacy Sawicki, “The Large Scale Structure of f(R) Gravity,” *Phys. Rev. D* **75**, 044004 (2007), arXiv:astro-ph/0610532.
- [33] Wayne Hu and Ignacy Sawicki, “Models of f(R) Cosmic Acceleration that Evade Solar-System Tests,” *Phys. Rev. D* **76**, 064004 (2007), arXiv:0705.1158 [astro-ph].
- [34] Levon Pogosian and Alessandra Silvestri, “The pattern of growth in viable f(R) cosmologies,” *Phys. Rev. D* **77**, 023503 (2008), [Erratum: Phys. Rev. D 81, 049901 (2010)], arXiv:0709.0296 [astro-ph].
- [35] Alireza Hojjati, Levon Pogosian, Alessandra Silvestri, and Starla Talbot, “Practical solutions for perturbed f(R) gravity,” *Phys. Rev. D* **86**, 123503 (2012), arXiv:1210.6880 [astro-ph.CO].
- [36] Marco Raveri, Bin Hu, Noemi Frusciante, and Alessandra Silvestri, “Effective Field Theory of Cosmic Acceleration: constraining dark energy with CMB data,” *Phys. Rev. D* **90**, 043513 (2014), arXiv:1405.1022 [astro-ph.CO].
- [37] Zhuangfei Wang, Seyed Hamidreza Mirpoorian, Levon Pogosian, Alessandra Silvestri, and Gong-Bo Zhao, “New MGMCAMB tests of gravity with CosmoMC and Cobaya,” *JCAP* **08**, 038 (2023), arXiv:2305.05667 [astro-ph.CO].
- [38] Alireza Hojjati, Levon Pogosian, and Gong-Bo Zhao, “Testing gravity with CAMB and CosmoMC,” *JCAP* **08**, 005 (2011), arXiv:1106.4543 [astro-ph.CO].
- [39] Tommaso Giannantonio, Matteo Martinelli, Alessandra Silvestri, and Alessandro Melchiorri, “New constraints on parametrised modified gravity from correlations of the CMB with large scale structure,” *JCAP* **04**, 030 (2010), arXiv:0909.2045 [astro-ph.CO].
- [40] Linfeng Xiao, Andre A. Costa, and Bin Wang, “Forecasts on interacting dark energy from the 21-cm angular power spectrum with BINGO and SKA observations,” *Mon. Not. Roy. Astron. Soc.* **510**, 1495–1514 (2021), arXiv:2103.01796 [astro-ph.CO].
- [41] T. Chen, R. A. Battye, A. A. Costa, C. Dickinson, and S. E. Harper, “Impact of $1/f$ noise on cosmological parameter constraints for SKA intensity mapping,” *Mon. Not. Roy. Astron. Soc.* **491**, 4254–4266 (2020), arXiv:1907.12132 [astro-ph.CO].
- [42] Philip Bull, Pedro G. Ferreira, Prina Patel, and Mario G. Santos, “Late-time cosmology with 21cm intensity mapping experiments,” *Astrophys. J.* **803**, 21 (2015), arXiv:1405.1452 [astro-ph.CO].
- [43] Kiyoshi Wesley Masui, Fabian Schmidt, Ue-Li Pen, and Patrick McDonald, “Projected Constraints on Modified Gravity Cosmologies from 21cm Intensity Mapping,” *Phys. Rev. D* **81**, 062001 (2010), arXiv:0911.3552 [astro-ph.CO].
- [44] Jacobo Asorey, Martin Crocce, Enrique Gaztanaga, and Antony Lewis, “Recovering 3D clustering information with angular correlations,” *Mon. Not. Roy. Astron. Soc.* **427**, 1891 (2012), arXiv:1207.6487 [astro-ph.CO].